Applied Surface Science 488 (2019) 107–114

Contents lists available at ScienceDirect

Applied Surface Science

journal homepage: www.elsevier.com/locate/apsusc

Full length article

Probing proximity effects in the ferromagnetic semiconductor EuO

Dmitry V. Averyanov[a], Andrey M. Tokmachev[a], Oleg E. Parfenov[a], Igor A. Karateev[a], Ivan S. Sokolov[a], Alexander N. Taldenkov[a], Mikhail S. Platunov[b], Fabrice Wilhelm[b], Andrei Rogalev[b], Vyacheslav G. Storchak[a,*]

[a] National Research Center "Kurchatov Institute", Kurchatov Sq. 1, Moscow 123182, Russia
[b] European Synchrotron Radiation Facility (ESRF), 38054 Grenoble Cedex, France

ARTICLE INFO

Keywords:
EuO
Gd
Ferromagnetism
Proximity effect

ABSTRACT

Ferromagnetic insulators are widely employed to induce magnetic phenomena in adjacent layers *via* proximity effect. This approach could make non-magnetic materials (ranging from silicon to graphene) available for spintronic applications. Eu chalcogenides, EuO in particular, are highly efficient spin generators but suffer from low Curie temperatures. Here, experiments aimed at T_C increase in EuO by its integration with the ferromagnetic metal Gd are reported. The epitaxial bilayers Gd/EuO are synthesized on different substrates and characterized by a combination of diffraction and microscopy techniques. Their magnetic structure – established with magnetization and transport measurements as well as element-selective X-ray magnetic circular dichroism study – comprises coupled magnetic orders of EuO and Gd. EuO is robust against proximity effects – its T_C is still low, increased at most by a few tens of K. Nevertheless, the results encourage further studies of proximity-enhanced ferromagnetism to extend the range of applications of ultrathin layers of EuO in spintronics.

1. Introduction

As materials dimensions are pushed down towards the nanoscale, the role of the interfaces is increasingly recognized [1]. Coupling of materials with different properties may bring fundamental changes to each of them. In particular, magnetic materials driving spin-related phenomena in adjacent layers are technologically important [2]. Magnetic order can be induced by proximity to any type of ferromagnet (FM); however, the use of insulating FM systems is strongly preferable since they do not shunt away currents in the target material. In addition, insulating FM systems can be highly efficient in spin tunneling applications. Regretfully, the selection of FM insulators (and semiconductors) is thin to say the least. Most such systems in use are formed by complex Fe-based oxides. Among them, the ferrimagnetic yttrium-iron garnet $Y_3Fe_5O_{12}$ is widely employed to establish magnetization dynamics in graphene [3,4], topological insulators [5], transition metal dichalcogenides [6], normal metals [7]. Structurally simpler ferrites such as $BiFeO_3$ and the spinel family ($CoFe_2O_4$, $NiFe_2O_4$) are also promising materials for spin manipulation *via* proximity exchange fields in 2D materials [8,9] and metals [10].

However, other FM insulators gain importance. In particular, layered 2D ferromagnets are especially useful once a control over valley splitting and spin polarization in monolayers is sought-after [11]. Eu chalcogenides (EuX) – a renowned class of magnetic semiconductors – induce strong proximity effects when coupled with graphene [12–14], topological insulators [15,16], other 2D materials [17]. EuO integrated with graphene is a prospective material for spin-based devices [18,19]. Successful integration of EuO with the mature Si technological platform [20,21] holds promise for silicon spintronics [22]. Equally enticing are theoretical predictions suggesting the use of EuO [23] or EuS [24] to induce spin effects in Mo dichalcogenides as well as formation of a spin-polarized 2D electron gas at the interface of EuO with an insulator [25,26].

The emerging importance of Eu chalcogenides in spintronic structures owes much to their robust Heisenberg-type magnetism with high magnetic moments provided by strongly localized 4*f*-shells (f^7) but also to superb interfaces formed by Eu chalcogenides with different materials [15,21]. Remarkably, deposition of EuS on graphene leads to a substantial increase in the carrier mobility [27]. The simple rock-salt structure of EuX is a strong advantage in both synthesis of nanostructures and their theoretical analysis. Being a relatively heavy element, europium can induce spin-orbit coupling in adjacent layers thus providing new opportunities in control over their electronic/magnetic states. EuO proves to be a particularly remarkable material: its enormous exchange splitting (0.6 eV) ensures spin polarization close to 100% [28] inviting a wide spectrum of spintronic applications. In the

* Corresponding author.
E-mail address: mussr@triumf.ca (V.G. Storchak).

https://doi.org/10.1016/j.apsusc.2019.05.191
Received 7 March 2019; Received in revised form 13 May 2019; Accepted 16 May 2019
Available online 21 May 2019
0169-4332/

bulk, EuO undergoes a prominent metal-insulator transition (MIT) [29]; it exhibits a colossal magnetoresistivity effect (6 orders of magnitude in a modest field of 2 T [29]) as well as very strong magneto-optic effects, exceptional sensitivity of magnetic and transport properties to strain, doping and optical pumping [30–33]. A recent study of the magnetic metal-insulator transition in EuO reveals a record MIT among thin films (up to 10 orders of magnitude in conductivity) as well as significant memory effects [32], associated with magnetic polarons. Furthermore, the topological Hall effect in doped EuO suggests the presence of skyrmions [34]. Remarkably, certain properties of EuX can be strongly enhanced by going to the nanoscale where size, shape and self-assembly of the particles can be varied [35]; synthesis of EuO nanotubes [36] aimed at magnetic vortex states with alternating chirality is an important recent breakthrough in this direction.

However, an important disadvantage of Eu chalcogenides is a rather low Curie temperature T_C (~17 K for EuS and ~69 K for EuO). Doping by trivalent atoms or creation of oxygen vacancies can lead to a significant increase of the Curie temperature; however, the process is accompanied by orders of magnitude increase in the carrier density [31,32] and the advantage of EuO being a semiconductor is irretrievably lost. Occasionally, Eu chalcogenides induce magnetic phenomena at temperature well above their T_C, as demonstrated in the EuS/Bi_2Se_3 [15] and EuO/graphene [14] structures. However, the cases are rare (applied specifically to 2D materials) and the high-temperature magnetism is more likely to be induced by spin-orbit coupling than by exchange interactions.

A viable alternative is to increase the Curie temperature of EuX itself by its coupling to an FM metal which supports FM at higher temperatures. This approach is implemented in element-selective studies of magnetism in *multilayers* of EuS/Co [37,38] and EuS/Ni [39] employing X-ray magnetic circular dichroism (XMCD) [37,39] and polar magneto-optic Kerr effect [38]. The studies demonstrate an antiparallel magnetic coupling between the adjacent layers leading to a fraction of EuS being FM at room temperature, which can be important for spintronic applications. The use of multilayers in such experiments raises a question of the magnetism location: only the outermost layer of EuS is important to applications based on the proximity effect but the high-temperature magnetism can be restricted to irrelevant central layers of EuS in the multilayer structure EuS/(FM metal). It calls for studies of simple bilayer structures where attribution of magnetism is more straightforward. In addition, attempts to increase the Curie temperature of EuO by an FM metal are yet to be reported although integration of EuO with metals does not pose problems as demonstrated by studies of Al/EuO (to make a superconductor with internal magnetization) [40], Nb/EuO (for enhanced magnetoresistance and metal-insulator transition) [41], Pt/EuO (for studies of surface-induced effects) [42] and Eu/EuO (for antiferromagnetic spintronics) [43].

Here, the FM semiconductor EuO is coupled with the FM metal Gd, which is known to grow epitaxially on many substrates. The bilayers comprising these 4*f* magnetic materials are produced on yttria-stabilized zirconia (YSZ) and silicon, employing molecular beam epitaxy. The structure of the films is characterized with electron and X-ray diffraction as well as electron microscopy to reveal formation of the face-centered cubic (*fcc*)-Gd interfaced with EuO. Magnetic properties of the films are determined with magnetization, electron transport and element-selective XMCD measurements. The potential of Gd to increase the effective Curie temperature of EuO *via* proximity effects is evaluated.

2. Experimental

2.1. Synthesis

The synthesis of all structures is carried out in a Riber Compact 12 system for molecular beam epitaxy. It operates in ultra-high vacuum which is established by a close-circle cryopump, a TiTan ion pump, a Titanium sublimation pump and cryopanels cooled by liquid N_2. The base pressure in the growth chamber does not exceed 10^{-10} Torr. The system is capable to maintain stable ratios of molecular beams without accumulation of reactants in the growth chamber. Molecular beams of 4 N Eu and 4 N Gd are supplied by heating the corresponding effusion cells. 6 N O_2 flux is tuned with a feedback-equipped gas flow system comprising a mass flow controller, a Baratron manometer and a mass spectrometer. Cells and substrate temperatures are controlled with thermocouples; the absolute temperature of the substrates is measured with an infrared pyrometer (PhotriX ML-AAPX/090) operating at the 0.9 μm wavelength. A Bayard-Alpert ionization gauge monitors the actual flux of molecular beams at the substrate site.

Two types of substrates are used in the synthesis: yttria-stabilized zirconia and silicon crystals. In both cases, orientation of the substrate wafers is (001), their thickness is 0.5 mm, and the miscut angle does not exceed 0.5°. The YSZ substrate is prepared by half an hour annealing at 600 °C in an oxygen atmosphere ($3\cdot10^{-8}$ Torr). The growth of EuO on YSZ(001) involves formation of a nucleation layer (5 monolayers) by deposition of europium ($3\cdot10^{-8}$ Torr) on the oxygen-saturated YSZ substrate at 430 °C. The rest of the film is grown by co-deposition of Eu ($1.2\cdot10^{-7}$ Torr) and O_2 ($6\cdot10^{-9}$ Torr) at 430 °C [32]. The synthesis of EuO on Si(001) is quite different [20,21]. The natural oxide is removed from the surface by heating up to 950 °C. The Si surface reconstructs to form a (2 × 1) superstructure. When exposed to a flux of Eu at 660 °C, it transforms into a metal-rich (1 × 5) structure [44]. Then, EuO films are grown at 340 ± 10 °C by reaction of Eu ($6\cdot10^{-8}$ Torr) and O_2 ($6\cdot10^{-9}$ Torr). In both cases of EuO/YSZ(001) and EuO/Si(001), the Gd layer is grown by metal deposition ($7\cdot10^{-8}$ Torr) at room temperature. Capping the films with 20 nm of amorphous SiO_x at room temperature prevents their degradation by ambient oxygen.

2.2. Structural characterization

The surfaces of the substrate, superstructures, films of EuO and gadolinium during the growth are controlled *in situ* employing reflection high-energy electron diffractometer (RHEED) equipped with the kSA 400 analytical RHEED system. The structure of the samples is further characterized with X-ray diffraction (XRD). The corresponding θ-2θ scans are recorded with a Rigaku Smartlab 9 kW diffractometer using a CuK_α X-ray radiation source. The specimens for microscopic studies are prepared in a Helios scanning electron microscope/focused ion beam (FIB) dual beam system which is equipped with gas injectors for Pt and C deposition and a micromanipulator. The major steps of the process are (i) deposition of a Pt layer (~2 μm); (ii) FIB milling with 30 keV Ga^+ ions till 2 μm-thick cross-sections with an area 8 × 5 μm^2 are formed; (iii) their attachment to the Omniprobe semiring; (iv) further thinning with 5 keV Ga^+ ions; (v) final cleaning with 2 keV Ga^+ ions till electron transparency. The cross-sections are analyzed with a 300 kV TEM/STEM Titan 80-300 microscope equipped with high-angle annular dark-field (HAADF) and bright-field detectors, a post-column Gatan energy filter, an atmospheric thin-window energy dispersive X-ray spectrometer and a spherical aberration (Cs) corrector. The resulting images are analyzed with Tecnai Imaging and Analysis and Digital Micrograph software.

2.3. Magnetic and transport properties

The macroscopic magnetic properties of the films are studied with a Quantum Design MPMS XL-7 SQUID magnetometer using two modes – reciprocating sample option and alternating current (AC). The samples are mounted in plastic straw; orientation of the film with respect to the external magnetic field is kept with accuracy better than 5°. XMCD studies are carried out at the European Synchrotron Radiation Facility ID12 beamline equipped with a fixed exit Si⟨111⟩ double crystal monochromator. Circularly polarized X-rays (the polarization rate exceeds 92%) are produced with a helical undulator of the APPLE-II type

with a magnetic period of 38 mm. The X-ray absorption and XMCD spectra at the L_3 absorption edge are recorded using the total fluorescence yield detection mode in the backscattering geometry. The SiO_x/Gd/EuO/YSZ(001) and SiO_x/Gd/EuO/Si(001) structures are fixed (with GE Varnish) at the cold finger of a He continuous-flow cryostat placed in the cold bore of a superconducting magnet. The XMCD experiments are carried out for two angles between the applied magnetic field and the sample surface – 15° and 90°. Repetitive measurements with the two opposite directions of the external magnetic fields up to 17 T ensure the XMCD spectra to be free of experimental artefacts. The spectra are typical for Gd films and for Eu chalcogenides reflecting magnetism of each layer separately. Measurements of the amplitude of XMCD signals as a function of the applied magnetic field provide the so-called element selective magnetization curves.

The electron transport in the films is studied in the van der Pauw configuration with a LakeShore 9709A Hall effect measurement system in the temperature range 2–300 K and magnetic fields up to 9 T. Deposition of an Ag-Sn-Ga alloy ensures Ohmic contacts to each terminal.

3. Results and discussion

3.1. Synthesis

Synthesis of EuO is not a trivial task since Eu(II) is an intermediate oxidation state of Eu. There always exists a risk of over-oxidation resulting in higher Eu oxides – Eu_3O_4 and Eu_2O_3. Moreover, both Eu and O_2 can react with substrates such as Si. In the synthesis, we rely on our extensive experience of EuO integration with different substrates [20,21,32]. Our method of choice is molecular beam epitaxy (MBE), not the least because the resistivity change at the metal-insulator transition in the best MBE films is 5 orders of magnitude larger than in the best non-MBE films [32,45]. We note, however, that stoichiometric EuO films produced by versatile pulsed laser deposition also demonstrate useful properties [46]. The EuO growth on YSZ(001) and Si(001) – the substrates we employ – requires quite distinct procedures and conditions. Zirconia stabilized with 13 molar % of yttria is chemically inert and lattice-matched with EuO: a(YSZ) = 5.147 Å while a (EuO) = 5.144 Å. However, it contains weakly bound oxygen – such an additional source of oxygen may jeopardize the growth. Therefore, the oxygen supply from YSZ must be taken under control. This is done by saturation of YSZ with O_2 at an elevated temperature; then, the first 5 monolayers of EuO are grown by deposition of Eu to react with oxygen extracted from YSZ without any external oxygen supply [47]. The rest of the film is synthesized in the weak distillation mode ensuring the precise stoichiometry: slightly higher than stoichiometric flux of Eu prevents over-oxidation while high temperature guarantees re-evaporation of excessive Eu atoms from the surface. The final thickness of the EuO layer is about 2.5 nm. This layer is chosen to be relatively thin because the proximity effect from the adjacent Gd is expected to be short-ranged. It should be taken into consideration, however, that such confinement may affect properties of EuO itself, *e.g.* the substantially reduced Curie temperature [20,42,48].

The main obstacle for the growth of EuO on Si(001) is formation of SiO_x and the Eu silicide $EuSi_2$ in reactions of O_2 and Eu with the substrate. Therefore, protection of the Si surface and a low enough temperature are required for the growth. Our approach is to use metal-rich submonolayer templates, in particular the robust (1 × 5) reconstruction of Eu on Si(001) [21,44]. This superstructure suppresses chemical reactions at the interface to avoid formation of unwanted phases. As a result, this technique provides EuO/Si(001) structures with atomically sharp interfaces [21]. However, the EuO growth in the distillation mode should be avoided because of a high temperature required. Instead, we tune the substrate temperature, Eu and oxygen fluxes. As in the case of YSZ, a 2.5 nm thick layer of EuO is grown to facilitate the comparison. This thickness is sufficient for relaxation of the lattice from the Si to bulk EuO parameters [20]. Thus, we prepare nearly equivalent films of EuO on YSZ(001) and Si(001). The next step is to grow a layer of Gd, which is not as trivial as it may appear. Gadolinium exhibits a very high affinity to oxygen. Although Eu is no slouch either when it comes to bonding with oxygen, Gd is well capable of taking O away from the preformed EuO film. Indeed, our experiments show that Gd deposition under thermodynamically controlled conditions results in Eu puddles at the interface. Luckily, MBE is precisely the technique to grow films in the kinetically controlled mode. 8 nm thick films of Gd are grown employing a relatively high flux of Gd deposited at low (room) temperature. The Gd film can react with air oxygen. It is possible to protect Gd by a layer of its oxide – non-magnetic Gd_2O_3. However, we employ a more controllable way – deposition of insulating SiO_x as a capping layer.

3.2. Structural characterization

To the best of the authors' knowledge, synthesis of Gd/EuO bilayers has not been reported in the literature. Therefore, it is especially important to determine the Gd/EuO structure and the quality of the interface. The MBE system allows for control of the film surface *in situ* employing RHEED. RHEED images for EuO/YSZ(001) and Gd/EuO/YSZ (001) (Fig. 1) illustrate high structural quality of the EuO and Gd layers. The respective images for the structures on the Si(001) substrate – EuO/Si(001) and Gd/EuO/Si(001) – are quite similar to those presented in Fig. 1. Fig. 1a corresponds to a well-formed film of EuO [20] despite its small thickness. The image of the Gd surface (Fig. 1b) requires explanation since it does not correspond to the regular hexagonal close-packed (*hcp*) lattice of bulk Gd.

At the nanoscale, formation of alternative polymorphs could be anticipated – epitaxial stabilization by the lattice of a substrate is a strong driving force [49]. In the case of gadolinium, formation of the *fcc* lattice in ultrathin films is well documented [50]. The RHEED image in Fig. 1b corresponds to this *fcc*-Gd phase. However, the extracted lattice parameter a(*fcc*-Gd), 5.22(3) Å in Gd/EuO/YSZ(001) and 5.18(3) Å in Gd/EuO/Si(001) (the values are virtually the same within the

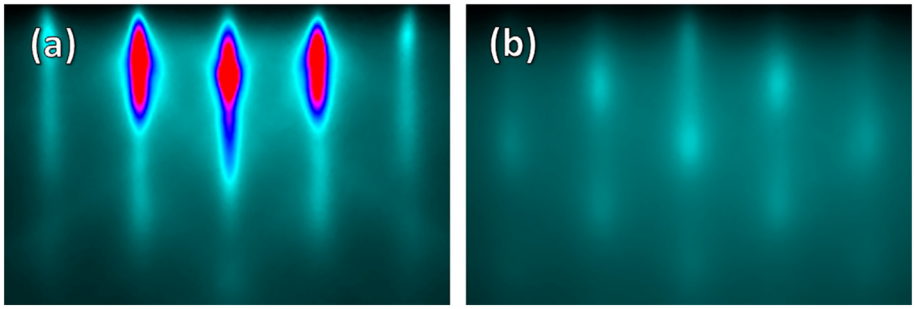

Fig. 1. RHEED images (along the [110] azimuth of EuO) of the SiO_x/Gd/EuO/YSZ(001) structure at different stages of the growth: (a) 2.5 nm of EuO are formed; (b) 8 nm of Gd on top of EuO are formed.

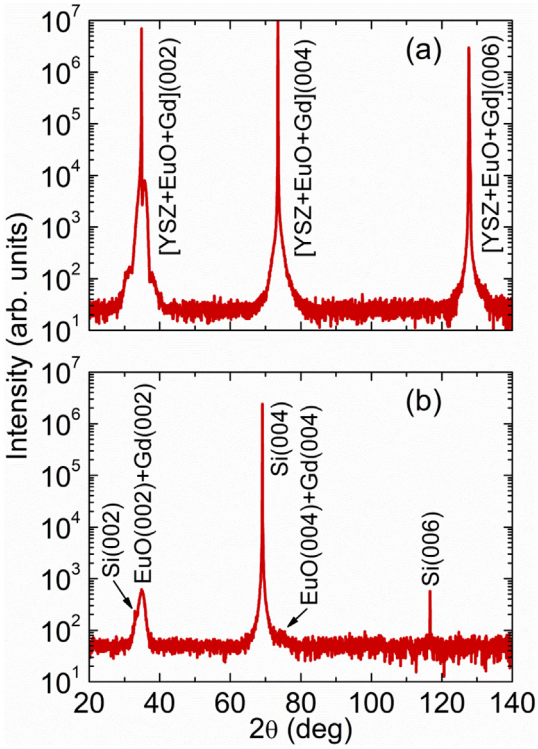

Fig. 2. θ-2θ X-ray diffraction scans of the structures (a) SiO_x/Gd/EuO/YSZ(001) and (b) SiO_x/Gd/EuO/Si(001).

experimental error), is noticeably smaller than the reported value *a*(*fcc*-Gd) = 5.32(1) Å [50]. Since *a*(*fcc*-Gd) in the Gd/EuO bilayer is closer to *a*(EuO) = 5.14 Å, it is likely that the lattice of *fcc*-Gd is soft enough to adjust for a reasonable lattice match with EuO.

The structure of the films is further studied *ex situ*. However, the match of the EuO and *fcc*-Gd lattices hinders interpretation of θ-2θ X-ray diffraction (XRD) scans (Fig. 2): the corresponding peaks from EuO and *fcc*-Gd overlap; in the case of SiO_x/Gd/EuO/YSZ(001), they are also eclipsed by the peaks from the substrate. The main result of the XRD study is that other phases of Gd (including *hcp*) do not show up. This is important since *fcc*-Gd is known to be pseudomorphic [50] – it undergoes an irreversible thickness-dependent transition to the more stable *hcp* phase. In fact, that is why we intentionally employ structures with a relatively thin (8 nm) layer of Gd.

Electron microscopy provides a better look into the atomic structure of the films; it also attests the quality of the interface. Fig. 3 presents high-resolution cross-sectional HAADF-STEM images of SiO_x/Gd/EuO/YSZ(001) and SiO_x/Gd/EuO/Si(001). Different zone axes are used to better illustrate the Gd lattice. The images confirm formation of *fcc*-Gd epitaxially coupled with EuO. Fast Fourier transforms for different areas (Fig. 3) help in identification of the phases. The extracted lattice parameter of *fcc*-Gd (5.21 Å, the same for the films on YSZ and Si substrates) is in a good agreement with the RHEED data. The interfaces Gd/EuO are atomically sharp which is highly important because the increase of the Curie temperature of EuO relies upon exchange coupling at this interface. The images do not reveal dislocations in Gd at the Gd/EuO interface. In addition, the electron microscopy study certifies the absence of any side phases. In particular, the EuO layer serves as a diffusion barrier preventing formation of the Gd silicide in the SiO_x/Gd/EuO/Si(001) structure, a compound which has recently been found to become FM once scaled to ultrathin layers [51–53].

3.3. Magnetic and transport properties

The ultimate goal for the synthesis of the Gd/EuO bilayers is to manipulate the magnetism of EuO. Therefore, studies of magnetic properties take center stage. The films are first characterized with magnetization (SQUID) measurements. This is an integral technique carrying information on the combined contributions from both EuO and Gd. The temperature dependence of the in-plane DC magnetic susceptibility *M*/*H* suggests appearance of ferromagnetism just below room temperature (Fig. 4a). It probably corresponds to the Curie temperature of *fcc*-Gd; however, the latter is a subject of some controversy in the literature [50] – depending on the source, *fcc*-Gd is thought to be a paramagnet or a ferromagnet with a variety of reported T_C. Perhaps, some difference in the lattice parameters, defects and/or film thickness causes such a discrepancy which can also be an element of a wider pattern of complex magnetism of Gd [54]. It is not easy to extract the magnetism of EuO from Fig. 4a – the curve is too complex to be quantitatively analyzed. The derivative $d(\ln M)/d(\ln T)$ exhibits local minima at 80 K and 113 K – very similar values are found for both SiO_x/Gd/EuO/YSZ(001) and SiO_x/Gd/EuO/Si(001). Although we cannot identify physical processes responsible for peculiarities observed at these temperatures (for example, whether they correspond to different layers of EuO), we couldn't help but notice that these two values are significantly higher than T_C of pristine EuO which in such ultrathin films falls around 50 K [42,48]. Magnetization measurements of SiO_x/EuO/Si(001) of the same thickness of the EuO layer as in SiO_x/Gd/EuO/Si(001) (Fig. 5) correspond to T_C(EuO) ≈ 48 K. Regretfully, we cannot measure magnetic properties of the corresponding individual Gd layer:

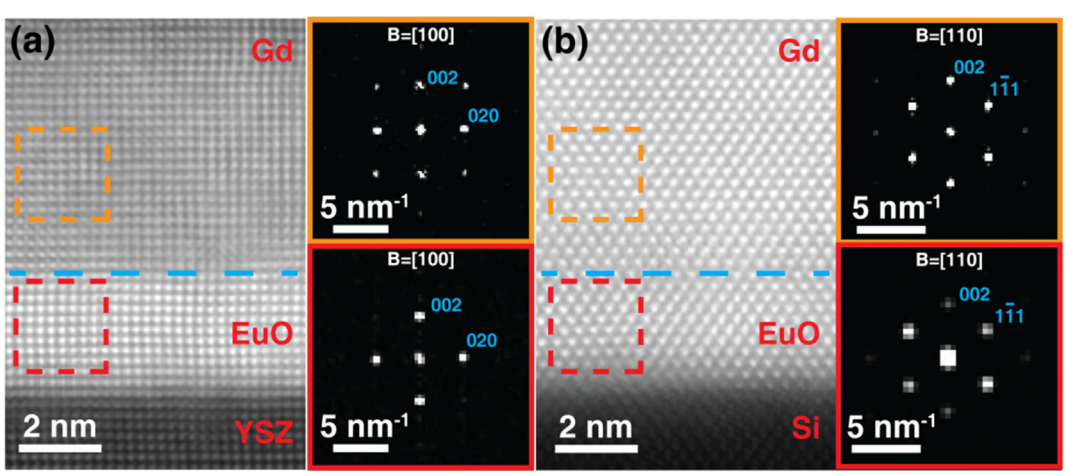

Fig. 3. High-resolution cross-sectional HAADF-STEM images of (a) SiO_x/Gd/EuO/YSZ(001) ([100] zone axis) and (b) SiO_x/Gd/EuO/Si(001) ([110] zone axis) structures. Insets show fast Fourier transform patterns from areas marked by red (EuO) and orange (Gd) squares. The interface is indicated by a dashed blue line.

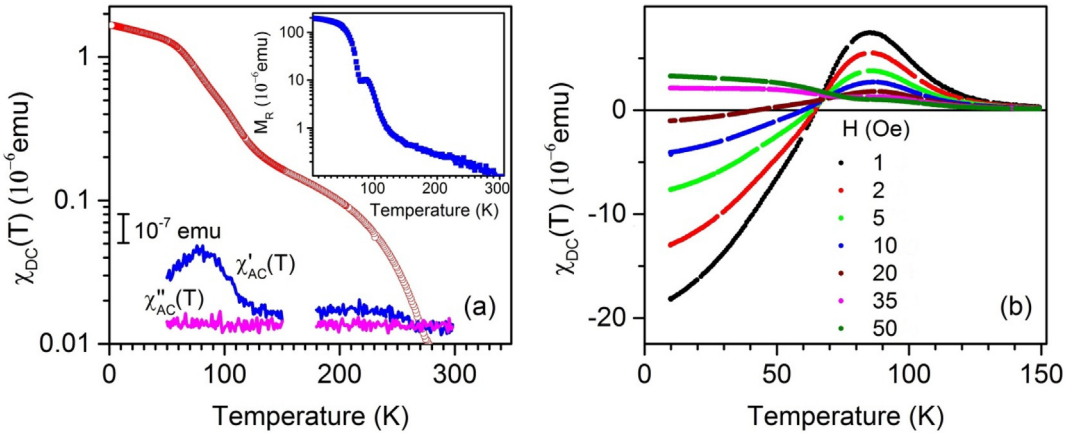

Fig. 4. (a) Temperature dependence of the in-plane DC magnetic susceptibility ($=M/H$) of the SiO_x/Gd/EuO/Si(001) structure (measured in 100 Oe), as well as the AC susceptibility components $\chi'(T)$ and $\chi''(T)$ (note the difference in the scales used). Inset: temperature dependence of the remnant moment of the SiO_x/Gd/EuO/YSZ(001) structure after cooling in 300 Oe. (b) Temperature dependence of the DC magnetic susceptibility of the SiO_x/Gd/EuO/YSZ(001) structure in low positive magnetic fields – 1 Oe (black), 2 Oe (red), 5 Oe (light-green), 10 Oe (blue), 20 Oe (brown), 35 Oe (magenta) and 50 Oe (dark-green).

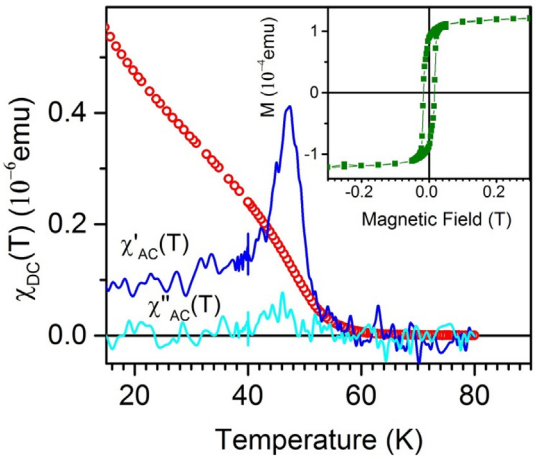

Fig. 5. Temperature dependence of the in-plane DC magnetic susceptibility ($=M/H$) of the SiO_x/EuO/Si(001) structure (measured in 100 Oe), as well as the AC susceptibility components $\chi'(T)$ and $\chi''(T)$. Inset: magnetic field dependence of the magnetic moment at 2 K.

(i) pseudomorphic *fcc*-Gd requires strong epitaxial stabilization; (ii) EuO stabilizes *fcc*-Gd with a very small lattice parameter – a condition which would be very difficult to reproduce with other substrates; (iii) Gd is highly reactive – forms silicides with Si [51–53] and oxide with YSZ – thus preventing epitaxial stabilization.

The non-trivial character of magnetism in the Gd/EuO bilayer is further confirmed by measurements of the remnant moment as well as AC susceptibility $\chi' + i\chi''$ (Fig. 4a). The low-temperature behavior of the total magnetic moment does not have any noticeable features. In particular, we do not detect an increase in magnetization characteristic to oxygen-deficient EuO [55] – it suggests that EuO does not depart significantly from its stoichiometry. Surprisingly, an anomalous increase of magnetization below 50 K, generally observed in thin films of Gd polymorphs and attributed to a spin reorientation effect [50], does not show up.

The magnetic response of the structures varies with the external magnetic field. Fig. 4b shows the DC magnetic susceptibility in the field cooled mode which strongly depends on the field – even its sign changes at low temperature. Such behavior may indicate a complex coupling at the Gd/EuO interface. In close analogy, an element-specific XMCD study of the Co/EuS multilayer structure demonstrates that the Eu magnetic moment is antiparallel to that of Co at remanence but rotates towards parallel alignment under an applied magnetic field [37]. However, such effect does not show up in $M - H$ loops. Instead, M

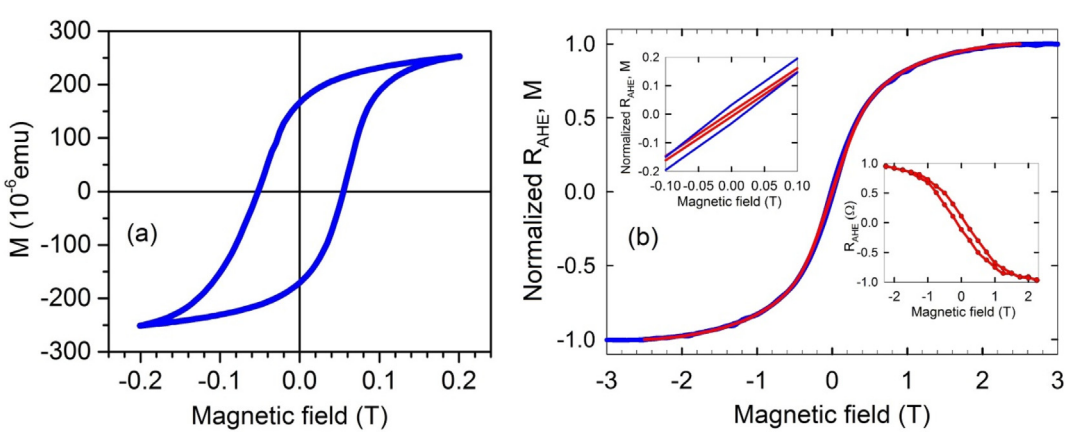

Fig. 6. (a) Magnetic field dependence of the magnetic moment of the SiO_x/Gd/EuO/Si(001) structure at 2 K. (b) Comparison of magnetic field dependences of the normalized anomalous Hall resistance R_{AHE} (red) and magnetic moment M (blue) of the SiO_x/Gd/EuO/YSZ(001) structure with a 20 nm layer of Gd at 100 K. Top-left inset: the low-field part of the dependences magnified. Bottom-right inset: magnetic field dependence of the anomalous Hall resistance of the SiO_x/Gd/EuO/Si(001) structure at 2 K.

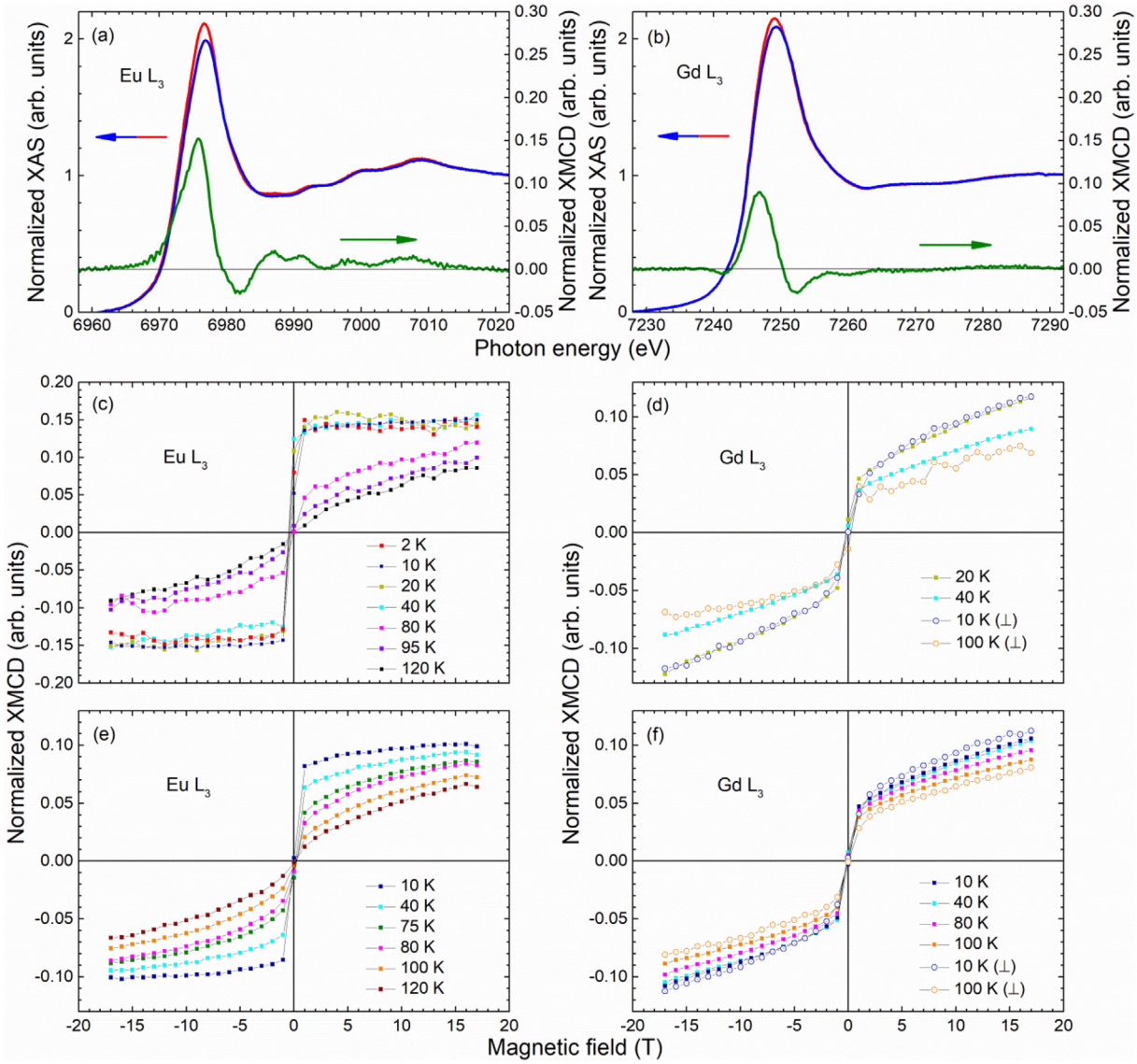

Fig. 7. Normalized XAS spectra for (a) Eu L_3 and (b) Gd L_3 absorption edges in the SiO_x/Gd/EuO/YSZ(001) structure in a magnetic field of 17 T at 2 K: right (red) and left (blue) circular polarizations; their difference (green) presents a normalized XMCD signal. Magnetic field dependence of the XMCD signal for the Eu and Gd L_3 absorption edges: (c) Eu and (d) Gd in the SiO_x/Gd/EuO/YSZ(001) structure; (e) Eu and (f) Gd in the SiO_x/Gd/EuO/Si(001) structure. The incidence angle is 15° or 90° (shown by the symbol ⊥).

(*H*) exhibits a hysteresis typical for FM systems (Fig. 6a). The characteristic coercive field (exceeding 500 Oe at 2 K) is not far from the value reported for *fcc*-Gd [50].

The FM order in the structures is further confirmed by electron transport measurements which demonstrate a pronounced anomalous Hall effect (AHE) with a hysteresis loop (bottom-right inset of Fig. 6b). The transport is dominated by metallic Gd; thus, the correspondence between magnetism and the Hall effect measurements can be established as soon as the EuO contribution is suppressed – we study Gd/EuO with a thick layer of Gd above T_C of EuO. Under these conditions, the normalized AHE resistance and out-of-plane magnetization almost coincide, besides somewhat different coercive fields (Fig. 6b). This result is a strong indication of the magnetic nature of the AHE in these structures.

The presented data are inconclusive with respect to the main question of T_C increase in the EuO layer. Element-selective studies are necessary to separate contributions from EuO and Gd, as in the case of EuS-based multilayers [37–39]. In particular, XMCD at the $L_{2,3}$ absorption edges of Eu has been proven useful [37,39]. Most XMCD studies of pristine EuO [56] and Gd-doped EuO [57] employ the $M_{4,5}$ absorption edges of Eu (and Gd). However, a recent XMCD study of Gd-doped EuO revealing the presence of magnetic polarons [32] suggests that the $L_{2,3}$ absorption edges provide a rather good insight into the magnetic state of EuO.

Fig. 7a,b presents typical X-ray absorption spectra (XAS) for the Eu and Gd L_3 absorption edges. The Eu spectra correspond to the Eu^{2+} species – no traces of Eu^{3+} contamination are detected – confirming once again the correct stoichiometry of the EuO films. The difference between the XAS spectra for right and left circular polarizations results in the respective XMCD signals. The magnetic field dependence of the normalized XMCD signals for the L_3 absorption edges of both Eu and Gd in the Gd/EuO bilayers is shown in Fig. 7c–f. First of all, we notice that the data for SiO_x/Gd/EuO/YSZ(001) and SiO_x/Gd/EuO/Si(001) are very similar. The magnetic response of Gd changes slightly as temperature goes up to 100 K. A remarkable fact is the absence of saturation for the Gd signal in magnetic fields as high as 17 T. It may be a sign of a complex magnetic structure of *fcc*-Gd, in analogy with *hcp*-Gd [54]. The Eu signal (reflecting the magnetic state of EuO) exhibits FM up to

80 K. The XMCD signal at 80 K amounts to about a third of the low temperature signal. It is difficult to make a comparison with the studies of EuS multilayers, which show the room temperature data only – the XMCD signal is reduced 14 times for Co/EuS [37] and more than 50 times for Ni/EuS [39] with respect to the low-temperature values. It should be noted that the Eu signal does not correspond to magnetic polarons because the characteristic saturation fields are too low [32]. Therefore, we believe the XMCD results reveal genuine changes in EuO magnetism. Regretfully, EuO turns out to be robust against proximity effects – T_C does not approach room temperature.

4. Conclusions

The modern spintronics relies upon the great number of magnetic materials gifted to us by nature. However, many materials of the uttermost importance, such as silicon, graphene or topological insulators, are non-magnetic. FM insulators fuse non-magnetic materials and spintronic applications by inducing spin polarization into the former. However, FM insulators are rare, their properties and application areas differ significantly. EuO is known for its simple atomic structure, robust Heisenberg-type ferromagnetism, high magnetic moments and extreme tunability of its properties. It would make an extraordinary spin injector if its T_C were not as low. Numerous attempts to increase T_C of EuO by doping sacrifice its insulating properties. In contrast, magnetic exchange coupling with an FM metal may increase the Curie temperature without making EuO a metal. Previous studies of EuS/(FM metal) multilayers suggest feasibility of such an approach. In the present work, we report synthesis, structural characterization and magnetic properties of the Gd/EuO bilayer on two different substrates – YSZ and Si. It is particularly interesting that Gd is stabilized in its metastable face-centered cubic form with a surprisingly small lattice parameter. Both integral magnetization and element-selective XMCD studies reveal a significant modification of magnetic properties of EuO. Although T_C of EuO is still low, not the least because T_C of Gd itself is below room temperature, the present work makes an important step forward towards high-temperature spin injectors based on EuO.

Acknowledgments

This work is partially supported by NRC “Kurchatov Institute” (synthesis), the Russian Foundation for Basic Research [grant 19-07-00249] (magnetization measurements), and the Russian Science Foundation [grant 19-19-00009] (transport measurements). The measurements have been carried out using the equipment of the resource centers of electrophysical, laboratory X-ray, and electron microscopy techniques of NRC “Kurchatov Institute”. The authors also gratefully acknowledge the beamtime allocation (MA-3167) by the ESRF.

References

[1] F. Hellman, A. Hoffmann, Y. Tserkovnyak, G.S.D. Beach, E.E. Fullerton, C. Leighton, A.H. MacDonald, D.C. Ralph, D.A. Arena, H.A. Dürr, P. Fischer, J. Grollier, J.P. Heremans, T. Jungwirth, A.V. Kimel, B. Koopmans, I.N. Krivorotov, S.J. May, A.K. Petford-Long, J.M. Rondinelli, N. Samarth, I.K. Schuller, A.N. Slavin, M.D. Stiles, O. Tchernyshyov, A. Thiaville, B.L. Zink, Interface-induced phenomena in magnetism, Rev. Mod. Phys. 89 (2017) 025006.
[2] P.K. Manna, S.M. Yusuf, Two interface effects: exchange bias and magnetic proximity, Phys. Rep. 535 (2014) 61–99.
[3] S. Sakai, S.V. Erohin, Z.I. Popov, S. Haku, T. Watanabe, Y. Yamada, S. Entani, S. Li, P.V. Avramov, H. Naramoto, K. Ando, P.B. Sorokin, Y. Yamauchi, Dirac cone spin polarization of graphene by magnetic insulator proximity effect probed with outermost surface spin spectroscopy, Adv. Funct. Mater. 28 (2018) 1800462.
[4] J.C. Leutenantsmeyer, A.A. Kaverzin, M. Wojtaszek, B.J. van Wees, Proximity induced room temperature ferromagnetism in graphene probed with spin currents, 2D Mater 4 (2017) 014001.
[5] Y.T. Fanchiang, K.H.M. Chen, C.C. Tseng, C.C. Chen, C.K. Cheng, S.R. Yang, C.N. Wu, S.F. Lee, M. Hong, J. Kwo, Strongly exchange-coupled and surface-state-modulated magnetization dynamics in Bi_2Se_3/yttrium iron garnet heterostructures, Nat. Commun. 9 (2018) 223.
[6] B. Peng, Q. Li, X. Liang, P. Song, J. Li, K. He, D. Fu, Y. Li, C. Shen, H. Wang, C. Wang, T. Liu, L. Zhang, H. Lu, X. Wang, J. Zhao, J. Xie, M. Wu, L. Bi, L. Deng, K.P. Loh, Valley polarization of trions and magnetoresistance in heterostructures of MoS_2 and yttrium iron garnet, ACS Nano 11 (2017) 12257–12265.
[7] J. Cramer, T. Seifert, A. Kronenberg, F. Fuhrmann, G. Jakob, M. Jourdan, T. Kampfrath, M. Kläui, Complex terahertz and direct current inverse spin Hall effect in YIG/$Cu_{1-x}Ir_x$ bilayers across a wide concentration range, Nano Lett. 18 (2018) 1064–1069.
[8] H.-D. Song, Y.-F. Wu, X. Yang, Z. Ren, X. Ke, M. Kurttepeli, G. van Tendeloo, D. Liu, H.-C. Wu, B. Yan, X. Wu, C.-G. Duan, G. Han, Z.-M. Liao, D. Yu, Asymmetric modulation on exchange field in a graphene/$BiFeO_3$ heterostructure by external magnetic field, Nano Lett. 18 (2018) 2435–2441.
[9] W. Jie, Z. Yang, F. Zhang, G. Bai, C.W. Leung, J. Hao, Observation of room-temperature magnetoresistance in monolayer MoS_2 by ferromagnetic gating, ACS Nano 11 (2017) 6950–6958.
[10] W. Amamou, I.V. Pinchuk, A.H. Trout, R.E.A. Williams, N. Antolin, A. Goad, D.J. O'Hara, A.S. Ahmed, W. Windl, D.W. McComb, R.K. Kawakami, Magnetic proximity effect in Pt/$CoFe_2O_4$ bilayers, Phys. Rev. Mater. 2 (2018) 011401 (R).
[11] D. Zhong, K.L. Seyler, X. Linpeng, R. Cheng, N. Sivadas, B. Huang, E. Schmidgall, T. Taniguchi, K. Watanabe, M.A. McGuire, W. Yao, D. Xiao, K.-M.C. Fu, X. Xu, Van der Waals engineering of ferromagnetic semiconductor heterostructures for spin and valleytronics, Sci. Adv. 3 (2017) e1603113.
[12] A.G. Swartz, P.M. Odenthal, Y. Hao, R.S. Ruoff, R.K. Kawakami, Integration of the ferromagnetic insulator EuO onto graphene, ACS Nano 6 (2012) 10063–10069.
[13] P. Wei, S. Lee, F. Lemaitre, L. Pinel, D. Cutaia, W. Cha, F. Katmis, Y. Zhu, D. Heiman, J. Hone, J.S. Moodera, C.-T. Chen, Strong interfacial exchange field in the graphene/EuS heterostructure, Nat. Mater. 15 (2016) 711–716.
[14] D.V. Averyanov, I.S. Sokolov, A.M. Tokmachev, O.E. Parfenov, I.A. Karateev, A.N. Taldenkov, V.G. Storchak, High-temperature magnetism in graphene induced by proximity to EuO, ACS Appl. Mater. Interf. 10 (2018) 20767–20774.
[15] F. Katmis, V. Lauter, F.S. Nogueira, B.A. Assaf, M.E. Jamer, P. Wei, B. Satpati, J.W. Freeland, I. Eremin, D. Heiman, P. Jarillo-Herrero, J.S. Moodera, A high-temperature ferromagnetic topological insulating phase by proximity coupling, Nature 533 (2016) 513–516.
[16] C. Lee, F. Katmis, P. Jarillo-Herrero, J.S. Moodera, N. Gedik, Direct measurement of proximity-induced magnetism at the interface between a topological insulator and a ferromagnet, Nat. Commun. 7 (2016) 12014.
[17] C. Zhao, T. Norden, P. Zhang, P. Zhao, Y. Cheng, F. Sun, J.P. Parry, P. Taheri, J. Wang, Y. Yang, T. Scrace, K. Kang, S. Yang, G. Miao, R. Sabirianov, G. Kioseoglou, W. Huang, A. Petrou, H. Zeng, Enhanced valley splitting in monolayer WSe_2 due to magnetic exchange field, Nat. Nanotech. 12 (2017) 757–762.
[18] Y. Song, G. Dai, Spin filter and spin valve in ferromagnetic graphene, Appl. Phys. Lett. 106 (2015) 223104.
[19] Y. Song, Y. Liu, X. Feng, F. Yan, W. Zhang, Spin-selectable, region-tunable negative differential resistance in graphene double ferromagnetic barriers, Phys. Chem. Chem. Phys. 20 (2018) 1560–1567.
[20] D.V. Averyanov, Y.G. Sadofyev, A.M. Tokmachev, A.E. Primenko, I.A. Likhachev, V.G. Storchak, Direct epitaxial integration of the ferromagnetic semiconductor EuO with silicon for spintronic applications, ACS Appl. Mater. Interf. 7 (2015) 6146–6152.
[21] D.V. Averyanov, C.G. Karateeva, I.A. Karateev, A.M. Tokmachev, A.L. Vasiliev, S.I. Zolotarev, I.A. Likhachev, V.G. Storchak, Atomic-scale engineering of abrupt interface for direct spin contact of ferromagnetic semiconductor with silicon, Sci. Rep. 6 (2016) 22841.
[22] L.L. Lev, D.V. Averyanov, A.M. Tokmachev, F. Bisti, V.A. Rogalev, V.N. Strocov, V.G. Storchak, Band structure of the EuO/Si interface: justification for silicon spintronics, J. Mater. Chem. C 5 (2017) 192–200.
[23] Q. Zhang, S.A. Yang, W. Mi, Y. Cheng, U. Schwingenschlögl, Large spin-valley polarization in monolayer $MoTe_2$ on top of EuO(111), Adv. Mater. 28 (2016) 959–966.
[24] X. Liang, L. Deng, F. Huang, T. Tang, C. Wang, Y. Zhu, J. Qin, Y. Zhang, B. Peng, L. Bi, The magnetic proximity effect and electrical field tunable valley degeneracy in MoS_2/EuS van der Waals heterojunctions, Nanoscale 9 (2017) 9502–9509.
[25] Y. Wang, M.K. Niranjan, J.D. Burton, J.M. An, K.D. Belashchenko, E.Y. Tsymbal, Prediction of a spin-polarized two-dimensional electron gas at the $LaAlO_3$/EuO (001) interface, Phys. Rev. B 79 (2009) 212408.
[26] K.J. Kormondy, L. Gao, X. Li, S. Lu, A.B. Posadas, S. Shen, M. Tsoi, M.R. McCartney, D.J. Smith, J. Zhou, L.L. Lev, M.-A. Husanu, V.N. Strocov, A.A. Demkov, Large positive linear magnetoresistance in the two-dimensional t_{2g} electron gas at the EuO/$SrTiO_3$ interface, Sci. Rep. 8 (2018) 7721.
[27] X. Zhang, L. Wei, R. Tao, X. Fan, L. Zhu, L. Cheng, L. Li, C. Zeng, Substantially enhanced carrier mobility in graphene in proximity to ferromagnetic insulator EuS, Appl. Phys. Expr. 10 (2017) 055103.
[28] P.G. Steeneken, L.H. Tjeng, I. Elfimov, G.A. Sawatzky, G. Ghiringhelli, N.B. Brookes, D.-J. Huang, Exchange splitting and charge carrier spin polarization in EuO, Phys. Rev. Lett. 88 (2002) 047201.
[29] T. Penney, M.W. Shafer, J.B. Torrance, Insulator-metal transition and long-range magnetic order in EuO, Phys. Rev. B 5 (1972) 3669–3674.
[30] N.J.C. Ingle, I.S. Elfimov, Influence of epitaxial strain on the ferromagnetic semiconductor EuO: first-principles calculations, Phys. Rev. B 77 (2008) 121202 (R).
[31] T. Mairoser, A. Schmehl, A. Melville, T. Heeg, L. Canella, P. Böni, W. Zander, J. Schubert, D.E. Shai, E.J. Monkman, K.M. Shen, D.G. Schlom, J. Mannhart, Is there an intrinsic limit to the charge-carrier-induced increase of the Curie temperature of EuO? Phys. Rev. Lett. 105 (2010) 257206.
[32] D.V. Averyanov, O.E. Parfenov, A.M. Tokmachev, I.A. Karateev, O.A. Kondratev, A.N. Taldenkov, M.S. Platunov, F. Wilhelm, A. Rogalev, V.G. Storchak, Fine structure of metal-insulator transition in EuO resolved by doping engineering,

Nanotechnology 29 (2018) 195706.
[33] M. Matsubara, A. Schroer, A. Schmehl, A. Melville, C. Becher, M. Trujillo-Martinez, D.G. Schlom, J. Mannhart, J. Kroha, M. Fiebig, Ultrafast optical tuning of ferromagnetism via the carrier density, Nat. Commun. 6 (2015) 6724.
[34] Y. Yun, Y. Ma, T. Su, W. Xing, Y. Chen, Y. Yao, R. Cai, W. Yuan, W. Han, Role of La doping for topological Hall effect in epitaxial EuO films, Phys. Rev. Mater. 2 (2018) 034201.
[35] X. Zhou, K.H.L. Zhang, J. Xiong, J.-H. Park, J.H. Dickerson, W. He, Size- and dimensionality-dependent optical, magnetic and magneto-optical properties of binary europium-based nanocrystals: EuX (X = O, S, Se, Te), Nanotechnology 27 (2016) 192001.
[36] B. Trepka, P. Erler, S. Selzer, T. Kollek, K. Boldt, M. Fonin, U. Nowak, D. Wolf, A. Lubk, S. Polarz, Nanomorphology effects in semiconductors with native ferromagnetism: hierarchical europium (II) oxide tubes prepared via a topotactic nanostructure transition, Adv. Mater. 30 (2018) 1703612.
[37] S.D. Pappas, P. Poulopoulos, B. Lewitz, A. Straub, A. Goschew, V. Kapaklis, F. Wilhelm, A. Rogalev, P. Fumagalli, Direct evidence for significant spin-polarization of EuS in Co/EuS multilayers at room temperature, Sci. Rep. 3 (2013) 1333.
[38] A. Goschew, M. Scott, P. Fumagalli, Verification of antiferromagnetic exchange coupling at room temperature using polar magneto-optic Kerr effect in thin EuS/Co multilayers with perpendicular magnetic anisotropy, Appl. Phys. Lett. 109 (2016) 062401.
[39] P. Poulopoulos, A. Goschew, V. Kapaklis, M. Wolff, A. Delimitis, F. Wilhelm, A. Rogalev, S.D. Pappas, A. Straub, P. Fumagalli, Induced spin-polarization of EuS at room temperature in Ni/EuS multilayers, Appl. Phys. Lett. 104 (2014) 112411.
[40] P.M. Tedrow, J.E. Tkaczyk, A. Kumar, Spin-polarized electron tunnelling study of an artificially layered superconductor with internal magnetic field: EuO-Al, Phys. Rev. Lett. 56 (1986) 1746–1749.
[41] A. Schmehl, D.G. Schlom, J. Mannhart, Increasing magnetoresistance using magnetic-field-tunable interfaces, Adv. Mater. 23 (2011) 1242–1245.
[42] M. Barbagallo, T. Stollenwerk, J. Kroha, N.-J. Steinke, N.D.M. Hine, J.F.K. Cooper, C.H.W. Barnes, A. Ionescu, P.M.D.S. Monteiro, J.-Y. Kim, K.R.A. Ziebeck, C.J. Kinane, R.M. Dalgliesh, T.R. Charlton, S. Langridge, Thickness-dependent magnetic properties of oxygen-deficient EuO, Phys. Rev. B 84 (2011) 075219.
[43] D.V. Averyanov, A.M. Tokmachev, O.E. Parfenov, I.A. Karateev, A.N. Taldenkov, V.G. Storchak, Coupling of magnetic orders in a 4f metal/oxide system, J. Mater. Chem. C 6 (2018) 9950–9957.
[44] D.V. Averyanov, C.G. Karateeva, I.A. Karateev, A.M. Tokmachev, M.V. Kuzmin, P. Laukkanen, A.L. Vasiliev, V.G. Storchak, A prospective submonolayer template structure for integration of functional oxides with silicon, Mater. Design 116 (2017) 616–621.
[45] D.G. Schlom, Perspective: oxide molecular-beam epitaxy rocks!, APL Mater 3 (2015) 062403.
[46] A. Mariscal, A. Quesada, A.T. Martín-Luengo, M.A. García, A. Bonanni, J.F. Fernández, R. Serna, Europium monoxide nanocrystalline thin films with high near-infrared transparency, Appl. Surf. Sci. 456 (2018) 980–984.
[47] R. Sutarto, S.G. Altendorf, B. Coloru, M. Moretti Sala, T. Haupricht, C.F. Chang, Z. Hu, C. Schüßler-Langeheine, N. Hollmann, H. Kierspel, H.H. Hsieh, H.-J. Lin, C.T. Chen, L.H. Tjeng, Epitaxial and layer-by-layer growth of EuO thin films on yttria-stabilized cubic zirconia (001) using MBE distillation, Phys. Rev. B 79 (2009) 205318.
[48] T.S. Santos, J.S. Moodera, K.V. Raman, E. Negusse, J. Holroyd, J. Dvorak, M. Liberati, Y.U. Idzerda, E. Arenholz, Determining exchange splitting in a magnetic semiconductor by spin-filter tunnelling, Phys. Rev. Lett. 101 (2008) 147201.
[49] A.M. Tokmachev, D.V. Averyanov, I.A. Karateev, O.E. Parfenov, O.A. Kondratev, A.N. Taldenkov, V.G. Storchak, Engineering of magnetically intercalated silicene compound: an overlooked polymorph of $EuSi_2$, Adv. Funct. Mater. 27 (2017) 1606603.
[50] T.P. Bertelli, E.C. Passamani, C. Larica, V.P. Nascimento, A.Y. Takeuchi, M.S. Pessoa, Ferromagnetic properties of fcc Gd thin films, J. Appl. Phys. 117 (2015) 203904.
[51] A.M. Tokmachev, D.V. Averyanov, O.E. Parfenov, A.N. Taldenkov, I.A. Karateev, I.S. Sokolov, O.A. Kondratev, V.G. Storchak, Emerging two-dimensional ferromagnetism in silicene materials, Nat. Commun. 9 (2018) 1672.
[52] O.E. Parfenov, A.M. Tokmachev, D.V. Averyanov, I.A. Karateev, I.S. Sokolov, A.N. Taldenkov, V.G. Storchak, Layer-controlled laws of electron transport in two-dimensional ferromagnets, Mater. Today (2019), https://doi.org/10.1016/j.mattod.2019.03.017.
[53] A.M. Tokmachev, D.V. Averyanov, A.N. Taldenkov, O.E. Parfenov, I.A. Karateev, I.S. Sokolov, V.G. Storchak, Lanthanide f^7 metalloxenes – a class of intrinsic 2D ferromagnets, Mater. Horiz. (2019), https://doi.org/10.1039/c9mh00444k.
[54] J.M.D. Coey, V. Skumryev, K. Gallagher, Is gadolinium really ferromagnetic? Nature 401 (1999) 35–36.
[55] P. Liu, J. Tang, Antiferromagnetic coupling in EuO_{1-x}, Phys. Rev. B 85 (2012) 224417.
[56] E. Negusse, J. Dvorak, J.S. Holroyd, M. Liberati, T.S. Santos, J.S. Moodera, E. Arenholz, Y.U. Idzerda, Magnetic characterization of ultrathin EuO films with XMCD, J. Appl. Phys. 105 (2009) 07C930.
[57] H. Ott, S.J. Heise, R. Sutarto, Z. Hu, C.F. Chang, H.H. Hsieh, H.-J. Lin, C.T. Chen, L.H. Tjeng, Soft x-ray magnetic circular dichroism study on Gd-doped EuO thin films, Phys. Rev. B 73 (2006) 094407.